Journal of
Materials Chemistry A

Materials for energy and sustainability

Accepted Manuscript

This article can be cited before page numbers have been issued, to do this please use: T. Asefa, B. Thomas, B. Peng and X. Huang, *J. Mater. Chem. A*, 2024, DOI: 10.1039/D4TA02845G.

ROYAL SOCIETY OF CHEMISTRY

rsc.li/materials-a

View Article Online
DOI: 10.1039/D4TA02845G

ARTICLE

Improving the Electrocatalytic Activity of Cobalt Oxide with Bismuth for Acidic Oxygen Evolution Reaction

Belvin Thomas,[a] Bowen Peng,[b] Xiaoxi Huang,[c*] and Tewodros Asefa[a,b*]

Received 00th January 20xx,
Accepted 00th January 20xx

DOI: 10.1039/x0xx00000x

Abstract. Highly durable, low-cost electrocatalysts for acidic oxygen evolution reaction (OER) are very essential for the commercial success of proton exchange membrane-based water electrolysis. The catalysts currently available for this reaction are mainly based on noble metals such as iridium (Ir) and ruthenium (Ru), which are notoriously unstable under acidic OER conditions, besides their high cost. Herein, we demonstrate that the incorporation of the main group metal bismuth (Bi) in cobalt oxide improves the latter's overall catalytic activity towards acidic OER without reducing its stability. Among the Bi-doped cobalt oxide catalysts synthesized with different Co:Bi ratios, the one with Co:Bi ratio of 9:1, denoted Co_9BiO_x, exhibits the best performance with an overpotential of 540 mV at the current density of 10 mA cm^{-2} at pH 1. It is also reasonably durable for about 45 hours while driving the reaction at a current density of 5 mA cm^{-2}. X-ray photoelectron spectroscopic studies and density functional theory-based calculations indicate that the Bi sites in these materials serve as catalytically active sites for acidic OER. In addition, the versatility of Bi in enhancing the catalytic activity of transition metal oxides towards acidic OER is demonstrated with Bi-doped iron oxides and nickel oxides.

1. Introduction

The rising global temperature due to the large emission of carbon dioxide and other greenhouse gases into the atmosphere has been leading to weather pattern disruptions and more frequent and intense snowstorms, rainfalls, flooding, heat waves, and forest fires around the world. These issues are further exacerbated by some unexpected events such as the recent Canadian wildfires and their environmental impacts.[1, 2] All of these, thus, call for an urgent transition from fossil fuels to carbon-neutral, renewable energy sources for our primary energy needs.

In recent decades, although large investments have been made in renewable solar and wind-based energy production methods, the intermittent nature of these energy sources has limited their full potential use. This can technically be addressed by coupling these energy ssources with electrochemical water splitting to produce green hydrogen (H_2). This approach has been gaining great interest as the excess off-peak energy produced by these energy sources can be stored in the form of this chemical energy (i.e., H_2), which can then be transported and used to generate electricity with fuel cells or via combustion.[3]

One of the most sustainable methods to produce H_2 is through electrochemical water splitting in an electrolyzer via the hydrogen evolution reaction (HER) at the cathode and the oxygen evolution reaction (OER) at the anode. The HER, which is a two-electron reaction, is relatively simpler to perform compared with the OER, which involves four-electrons and is thus kinetically sluggish. The latter is also the main factor limiting the overall efficiency of water electrolyzers. The overall efficiency of electrochemical water splitting can further be affected by the media in which it is carried out. When water electrolysis in acidic medium is compared with one in alkaline medium, the former is generally a clear winner. As an example, proton exchange membrane water electrolyzers (PEMWEs), which work in acidic medium, have the advantage of having compact design, great power density, high efficiency at low temperature, partial load range, and low gas crossovers.[4-6] Additionally, the high proton concentrations in acidic media enables a faster HER than that in alkaline medium while the low Ohmic resistance due to the higher conductivity of hydronium ions (350 S cm^2 mol^{-1}) over hydroxide ions (198 S cm^2 mol^{-1}) creates a favorable condition for the overall process in them.[7, 8] To date, the state-of-the-art OER catalysts for acidic media are noble metal oxides, namely IrO_2 and RuO_2; however, their high cost, instability, and scarce availability limit their large-scale application for industrial PEMWEs.[9, 10] So, there is an urgent need to develop noble metal-free OER electrocatalysts that can catalyze the OER in acidic media while remaining stable.

While various electrocatalysts based on first-row transition metals that are stable and show catalytic activity for OER in alkaline media have been developed, most of them are highly unstable during OER in acidic media at high oxidation potentials.[11] Co- and Mn-oxides are among the few exceptions that have been the target of many studies focusing on the development of effective, acid-stable OER catalysts.[12-18] But, spinel cobalt oxide (Co_3O_4), which can catalyze OER, still suffers from low stability under harsh acidic conditions at

[a] Department of Chemistry and Chemical Biology, Rutgers, The State University of New Jersey, 610 Taylor Road, Piscataway, NJ, 08854, USA; E-mail: tasefa@chem.rutgers.edu
[b] Department of Chemical and Biochemical Engineering, Rutgers, The State University of New Jersey, 98 Brett Road, Piscataway, NJ, 08854, USA
[c] Hoffmann Institute of Advanced Materials, Shenzhen Polytechnic University, 7098 Liuxian Blvd, Nanshan District, Shenzhen, 518055, PR China; E-mail: xiaoxihuang@szpu.edu.cn

high oxidation potentials.[19] One approach that is applied to improve the stability and activity of this promising acid OER catalyst involves doping it with other elements such as metals. For example, the overall conductivity, stability, and electrocatalytic activity of spinel Co_3O_4 nanowires for OER in acid media were improved by doping them with Ag.[20] Similarly, when cobalt oxide (CoO_x) was doped with Fe and Pb atoms, producing $CoFePbO_x$, the material exhibited higher stability during OER in acidic solution than CoO_x while maintaining its high catalytic activity for the reaction.[11] Another approach applied to improve the stability of Co_3O_4 is using an acid-stable protective layer, such as carbon or TiO_2, to prevent the leaching of Co atoms from the material under such conditions.[21-23]

Other recent research reports have shown that coupling 3d transition metals (Mn/Fe/Co/Ni) with acid-stable oxides of Sb/Ti/Sn/Ge/Mo/W could yield effective OER catalysts for acidic media.[24-26] For example, TiO_2 was coupled with Mn/Co/Fe oxides to produce acid-stable OER catalysts.[27, 28] Similarly, Co_2TiO_4 and TiO_2-incorporated MnO_2 catalysts were shown to exhibit catalytic activity for OER for prolonged hours in highly acidic solutions.[13, 29] Metal oxides, such as SbO_x, were also demonstrated to generate acid durable OER catalysts. For example, the incorporation of Sb into $FeCoO_x$, which produces $FeCoSbO_x$, gives rise to more stable and efficient electrocatalysts for OER in acidic solutions.[30] $(Mn,Sb)O_2$ possessing rutile structure, pyrochlore-type $Co_2Sb_2O_7$, phase-pure $CoSb_2O_6$, and $MnSb_2O_6$ have also been shown to serve as stable OER catalysts with good activity and stability.[31, 32]

After the recent report on the stability of BiO_x under acidic conditions, there has been a growing interest in this p-block metal oxide for electrocatalysis applications.[33] For example, $[Ag+Bi]O_x$ and Co-Bi-SnO_x have successfully been demonstrated to catalyze the OER while remaining stable in acidic solution.[34, 35] The stability of these catalysts has been attributed to the stabilizing role of the acid-stable bismuth oxide matrix. BiO_x provides an added benefit in acidic OER electrocatalysis because it can sustain the reaction via the Bi^{3+}/Bi^{5+} oxidation states it forms at its Bi sites, which help with the formation of the hydroxo/peroxo intermediates needed for facile OER.[33] A recent study from our group also showed that Bi's oxophilic nature and ability to tune the electronic states in metal borates could be taken advantage to stabilize the OER intermediates and thereby to enhance OER catalysis.[36]

Herein we report petal-shaped Bi-doped cobalt oxides that are synthesized in situ on fluorine-doped tin oxide (FTO) substrates and their excellent electrocatalytic activity and durability during acidic OER. The catalysts are synthesized using a simple procedure wherein Co(II) and Bi(III) salts are mixed in citric acid solution, then drop-casted on FTO, and finally annealed. The catalytic active sites on the materials are comprised of thin layers of Bi-doped cobalt oxides that are deposited on FTO. The catalysts remain stable in 0.1 M $HClO_4$ solution for 24 hours while electrocatalyzing the OER at a current density of 5 mA cm^{-2}. The effects of the amounts of Bi dopants in cobalt oxides on the activity and stability of the catalysts towards acidic OER are investigated by varying the Co:Bi ratios in the materials and then testing their electrocatalytic activities for prolonged hours. Bi is also found to enhance the electrocatalytic activities of iron oxide and nickel oxide for OER. These findings may encourage the exploration of other p-block metals as dopants into various transition metal oxides for acidic OER electrocatalysis.

2. Results and discussion

Co_3O_4, Bi_2O_3, and Bi-doped Co_3O_4 catalysts with different Co:Bi ratios were synthesized in situ by depositing solutions of the respective metal ions in citric acid on FTO glass slides and then annealing them, as illustrated in the schematic in Figure 1. The Bi-doped Co_3O_4 catalysts obtained from the synthesis are named as $Co_aBi_bO_x$, such that a:b represents the mole ratios of Co(II):Bi(III) used for the synthesis of the catalysts, which are 14:1, 9:1, 2:1, and 1:2. Citric acid is added for the synthesis of these materials because the citrate it forms in the solution helps dissolve the metal salts and thus enable the metal ions mix uniformly.[37] Besides, the citrate groups can easily undergo decomposition into CO_2 and be removed during annealing, and leave behind pristine metal oxides on the FTO. A small amount of nitric acid is also included in the solution in order to help dissolve Bi(III) nitrate and prevent it from precipitating as $Bi(OH)_3$.[38]

The catalysts synthesized on FTO are characterized first by X-ray diffraction (XRD) (Figure 2 and S2). The XRD pattern obtained for pristine cobalt oxide on FTO shows peaks at 2θ = 19.04, 31.26, and 37.05°, which can be ascribed to the (111), (220), and (311) crystalline planes, respectively, of Co_3O_4 with spinel structure (based on the Joint Committee on Powder Diffraction Standard or JCPDS No.: 42-1467).[14] The XRD pattern also shows the diffraction peaks of the FTO substrate itself at 2θ = 26.5, 33.63, 37.72, 51.53, and 61.55. 65.51°. These peaks are also observed in all the other cases where

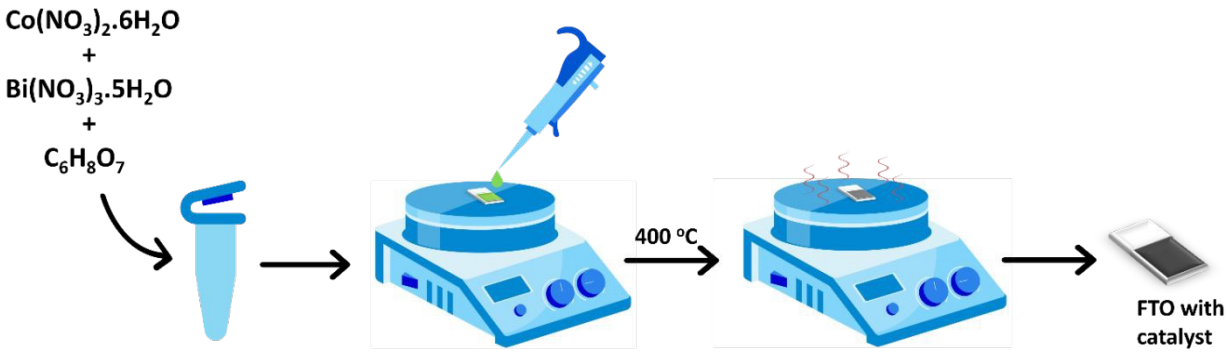

Figure 1. Schematic of the synthesis of $Co_aBi_bO_x$ catalysts on FTO. The precursor used as the source of Co(II) nitrate, Bi(III) nitrate, and citric acid in acid solution, followed by the deposition of the solution onto FTO substrates and annealing. Co_3O_4, $Co_{14}Bi_1O_x$, and $Co_9Bi_1O_x$ on FTO are examined, apart from the

View Article Online
DOI: 10.1039/D4TA02845G

ARTICLE

peaks corresponding to FTO, no peaks associated with spinel Co_3O_4 or Bi_2O_3 are seen on them. For example, the XRD pattern of $Co_{14}BiO_x$ on FTO shows only a faint peak at ~31° corresponding to the (220) plane of spinel Co_3O_4. This means that the XRD pattern of $Co_{14}BiO_x$ on FTO does not show the peaks associated with many crystalline planes of Co_3O_4, unlike that of pristine Co_3O_4 on FTO. These results indicate that incorporating Bi into Co_3O_4 results in materials that are largely amorphous. Additionally, a broad peak at 2θ of ~28° is seen in the XRD pattern of $CoBi_2O_x$, due to the amorphous feature Bi_2O_3 in it as Bi is the major metal in this material. It is worth noting here that the XRD pattern of pristine Bi_2O_3 on FTO (Figure S1) exhibits peaks due to α-Bi_2O_3 (JCPDS No.: 41-1449).[39] These mean that the in situ synthesis reported herein yields amorphous catalysts in the case of Bi-doped cobalt oxides but crystalline ones in the case of the pristine Co_3O_4 and Bi_2O_3.

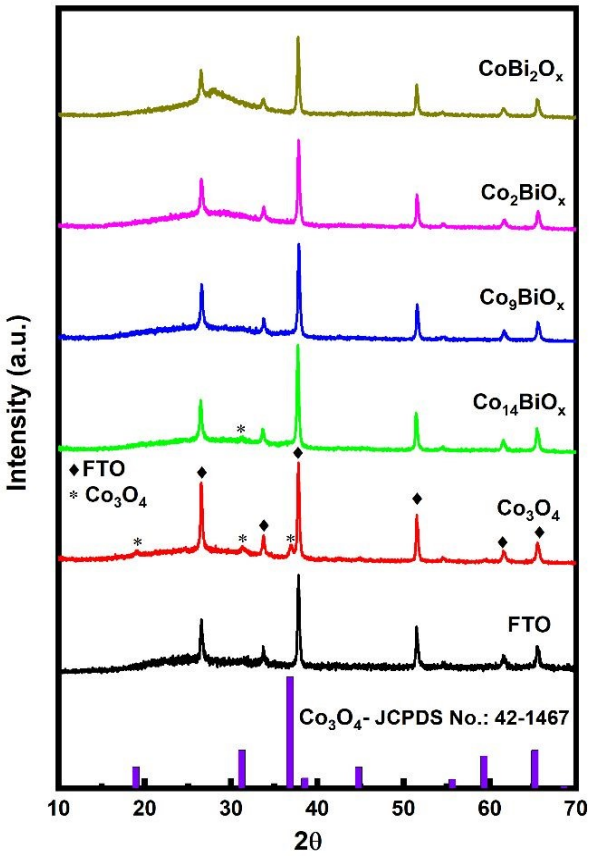

Figure 2. XRD patterns of FTO substrate and the different catalysts synthesized in situ on FTO substrates, namely Co_3O_4, $Co_{14}BiO_x$, Co_2BiO_x, and $CoBi_2O_x$. The JCPDS of Co_3O_4 is included for reference.

The field emission scanning electron microscopy (FESEM) images of Co_9BiO_x, which is the best performing catalyst (*vide infra*), are displayed in Figure 3a-c. The images exhibit that this material is composed of thin filament and petal shaped particles, just as those of the $CoMnO_x$ OER catalysts reported by Huynh et al.[11] In Figure S2, the material on FTO appears black in color, as seen in its digital image in Figure S2. The FESEM images of the other catalysts synthesized on FTO also exhibit similar morphologies (Figure S3 - S7a-c). However, upon examining the images further, these morphologies are more pronounced when the amount of Co in the catalysts is relatively higher. For instance, the petal-like morphology is best seen in the FESEM images of Co_3O_4, $Co_{14}BiO_x$, and Co_9BiO_x, which have higher Co:Bi ratios (Figure 3, S3-S4, and S6a-c). When the catalysts are made with higher amounts of Bi, they show thicker sheet-like structures (see, for example, the FESEM images of $CoBi_2O_x$ and Bi_2O_3 in Figures S5 and S7a-c). The energy dispersive X-ray spectroscopy (EDS) elemental mapping images of Co_9BiO_x (Figure 3d) show Co, Bi, and O that are distributed throughout the sample. Similarly, the EDS mapping images of all other Bi-doped cobalt oxides (Figure S3-S6d) show uniform distributions of Co, Bi, and O. The ratios of Co:Bi in the materials are also analyzed from these EDS mapping images, and they are found to be like the corresponding ratios of Co and Bi (in mol) used in the precursors to synthesize them (Table S1).

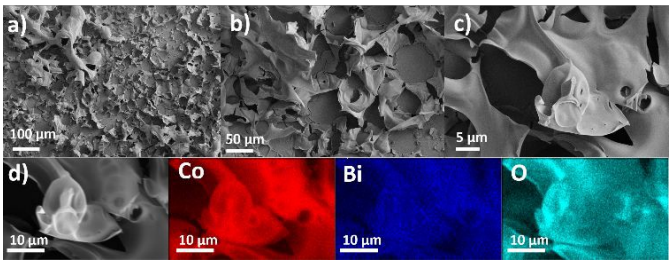

Figure 3. (a-c) FESEM images and (d) EDS elemental mapping images of Co_9BiO_x on FTO. The latter show that Co, Bi, and O are uniformly distributed on the catalyst.

X-ray photoelectron spectroscopy is applied to determine the surface atomic compositions and chemical states of the catalysts present on FTO. The XPS survey spectra show peaks corresponding to Co, Bi, O, and C and two other peaks corresponding to Sn and Si that originate from the FTO substrate (Figure S9). The high-resolution Co 2p XPS spectra of all the catalysts containing Co have two main broad peaks at binding energies of 780.0 and 795.0 eV, which correspond to the Co $2p_{3/2}$ and $2p_{1/2}$ states, respectively (Figure 4a). The high-resolution Co 2p XPS spectra show weak satellite peaks with higher binding energies around those of $2p_{3/2}$ and $2p_{1/2}$, which indicate the presence of Co^{2+} and Co^{3+} on the catalysts.[40] The $2p_{3/2}$ and $2p_{1/2}$ peaks in the high-resolution Co 2p XPS spectra are deconvoluted to determine the chemical states of Co on the surfaces of the catalysts. The deconvoluted Co $2p_{3/2}$ peaks of all Co-containing catalysts are seen at binding energies of ~779.5 and ~780.6 eV, and they are ascribed to Co^{3+} and Co^{2+} oxidation states, respectively. In the case of pristine cobalt oxide on FTO, the ratio of Co^{2+}:Co^{3+} calculated from its XPS spectrum is 3.67, although the XRD pattern

View Article Online
DOI: 10.1039/D4TA02845C

indicates that this material exists in spinel structure where the Co^{2+}:Co^{3+} ratio should be 0.5. This difference indicates the presence of a much larger amount of Co^{2+} species, and by extension, more oxygen vacancies, on the surfaces of the pristine cobalt oxide.[41] This is further corroborated based on the deconvoluted high resolution O 1s spectra of the material (see below). The deconvoluted O 1s XPS survey spectrum of pristine Co_3O_4 on FTO (Figure S10) displays peaks at 529.83 eV and 531.1 eV, which correspond to Co-O bond and oxygen vacancies (O_{vac}) or defect sites, respectively. The O 1s XPS survey spectra of all Bi-doped cobalt oxide catalysts on FTO (Figure S10) also indicate the presence of oxygen vacancies, which must be formed due to the decomposition of citrate groups into CO_2 during the annealing step of their syntheses. The decomposition of citrate from the materials into CO_2 generates the oxygen vacancies, with perhaps a similar process to the one previously reported for ligand-assisted polyol synthesis of cobalt oxide by using the polymer polyacrylic acid as a ligand.[43]

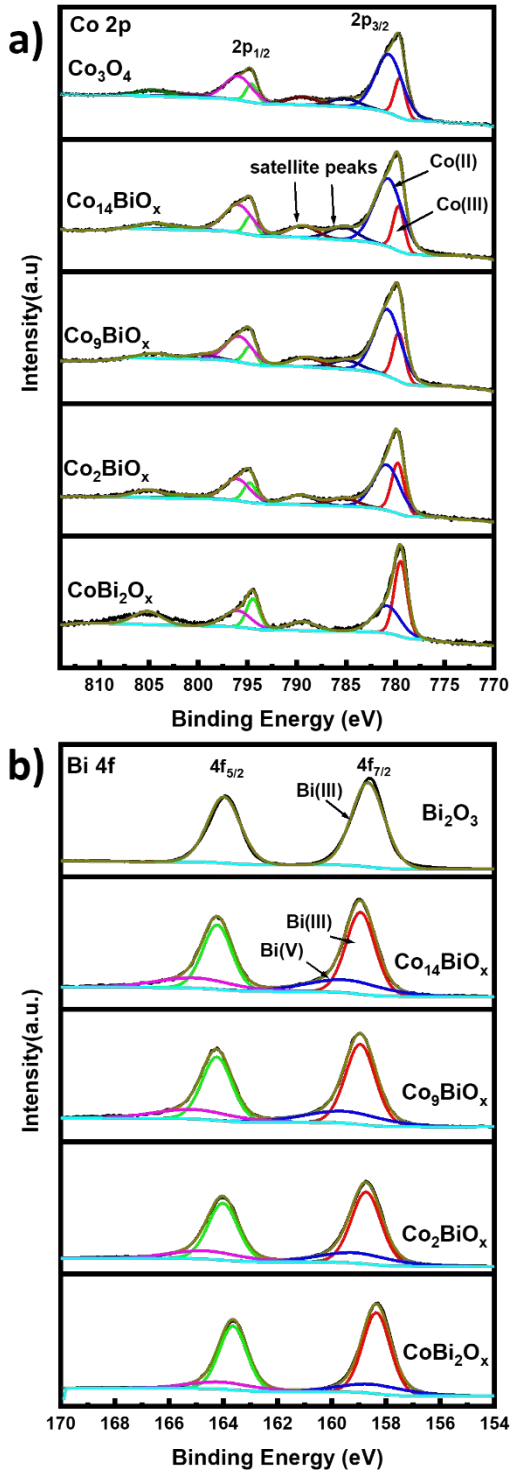

Figure 4. High resolution XPS spectra showing peaks corresponding to (a) Co 2p and (b) Bi 4f of Co_3O_4, $Co_{14}BiO_x$, Co_9BiO_x, Co_2BiO_x, $CoBi_2O_x$, and Bi_2O_3 catalysts.

Similarly, the deconvoluted Bi 4f XPS spectra of Bi in Bi-doped cobalt oxides on FTO (Figure 4b) show two sets of peaks: the first one at binding energies of 158.9 and 164.2 eV that can be attributed to Bi $4f_{7/2}$ and Bi $4f_{5/2}$ of Bi^{3+}, respectively, and the second one at 159.5 and 165.0 eV that can be ascribed to Bi $4f_{7/2}$ and Bi $4f_{5/2}$ of Bi^{5+}, respectively.[44] However, the high resolution Bi 4f XPS spectrum of pristine Bi_2O_3 on FTO shows only peaks at 158.67 and 163.97 eV corresponding Bi $4f_{7/2}$ and Bi $4f_{5/2}$ of Bi^{3+} species, respectively. These results indicate that Bi co-exists in two oxidation states (i.e., Bi^{3+} and Bi^{5+}) in the Bi-doped cobalt oxides on FTO, but only as Bi^{3+} in Bi_2O_3 on FTO.

Based on the XPS results, the relative amounts of Bi^{3+} and Bi^{5+} species with respect to the total amount of Bi in Bi-doped cobalt oxides are also determined (see Table S2). While the results indicate that the relative amount of Bi^{3+} is higher than that of Bi^{5+} in all Bi-doped cobalt oxide catalysts, the highest relative amount of Bi^{5+} species is obtained for $Co_{14}BiO_x$, which contains the lowest amount of Bi. In other words, the relative amount of Bi^{5+} increases as the amount of Bi in the Bi-doped cobalt oxides decreases. Additionally, the relative amounts of Co^{2+} and Co^{3+} in the Bi-doped cobalt oxides with respect to their Bi content are analyzed. In $Co_{14}BiO_x$, which has the lowest amount of Bi among the Bi-doped cobalt oxides, the amount of Co^{2+} species is 3.88 times higher than that of Co^{3+} species. On the other hand, when the amount of Bi in the catalysts is increases (e.g., $CoBi_2O_x$), Co exists increasingly more as Co^{3+} species rather than as Co^{2+} species. These results show that the amounts of Bi in Bi-doped cobalt oxide catalysts affect the oxidation states of both Bi and Co as well as their relative amounts in them. Using the XPS results, the Co:Bi mole ratios on the surfaces of all Bi-doped cobalt oxide catalysts are also determined and compiled in Table S2. The values match well with those used for the synthesis of the respective catalysts.

Raman spectroscopy is used to further confirm the presence of oxygen vacancies in the Bi-doped cobalt oxides synthesized on FTO. As shown in Figure S11, spinel Co_3O_4 shows five distinct Raman bands at 195.6, 481.5, 518.9, 615.2, and 683 cm^{-1}, which are respectively ascribed to the F2g, Eg, F2g, F2g, and A1g Raman active vibrational modes.[45, 46] Among them, the bands at 195.6 and 683 cm^{-1} are ascribed to the Co^{2+}-O^{2-} and Co^{3+}-O^{2-} Raman active vibrations, respectively. In the case of Co_3O_4 synthesized on FTO, the A1g mode is slightly blue-shifted (to 685 cm^{-1}), which is due to the O_{vc} present in Co_3O_4, as previously reported in the literature.[45,46] This showcases that oxygen vacancies are produced during the in-situ synthesis of the catalysts on FTO. Similarly, the A1g vibration mode is blue-shifted for the catalyst $Co_{14}BiO_x$ and Co_9BiO_x when compared with that of

View Article Online
DOI: 10.1039/D4TA02845G

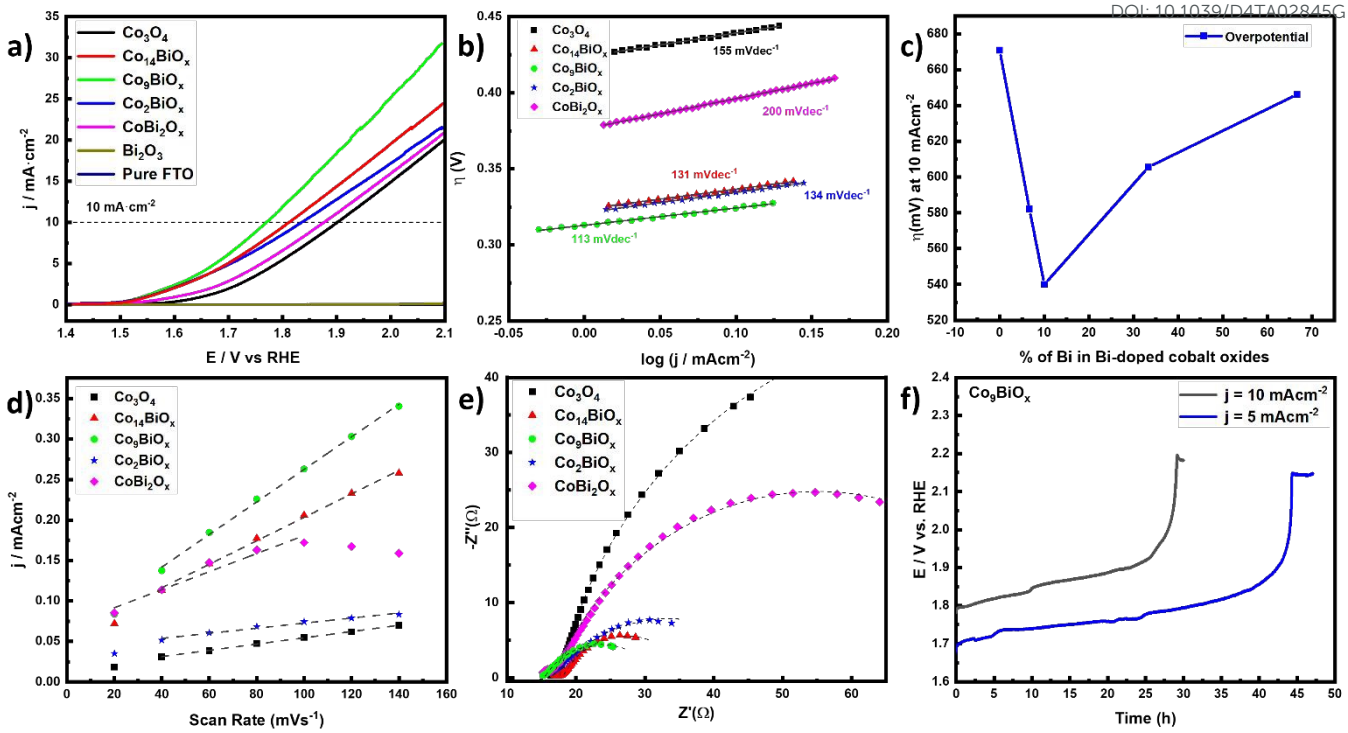

Figure 5. (a) The LSV curves obtained for OER as catalyzed by Co_3O_4, $Co_{14}BiO_x$, Co_9BiO_x, Co_2BiO_x, $CoBi_2O_x$, and Bi_2O_3 in 0.1 M $HClO_4$ solution at a scan rate of 5 mV s^{-1}. (b) The Tafel plots of the reactions catalyzed by the materials, which are derived from their respective LSV curves. (c) Plots of the overpotential required by the catalysts to drive OER at a current density (j) = 10 mA cm^{-2} versus the percentage of Bi in the catalysts. (d) Plots of the charging current obtained from the difference between the anodic and cathodic currents versus the scan rate in the non-faradaic region of OER, which are used to determine the capacitances of the catalysts. (e) Nyquist plots for Co_3O_4, $Co_{14}BiO_x$, Co_9BiO_x, Co_2BiO_x, and $CoBi_2O_x$ obtained from their respective EIS measurements. (f) Chronopotentiometry profiles obtained for Co_9BiO_x to determine its stability during electrocatalytic OER at current density j = 5 and 10 mA cm^{-2}.

spinel Co_3O_4. However, when the amounts of Bi in Bi-doped Co_3O_4 increases, the A1g vibrational mode of the catalyst is red-shifted to low vibrational frequencies. When very small amounts of Bi are doped into Co_3O_4, the A1g vibration mode is reported to show a blue shift, as a large ion such Bi^{3+} occupy the octahedral sites in Co_3O_4 by substituting Co^{3+} ions.[47] With the increase in the amount of Bi in cobalt oxide, the Co^{3+} ions at the octahedral sites will be replaced with Bi^{3+} ions, and this results in a dramatic red shift of A1g vibration mode of the catalysts. Additionally, the Raman bands between 450-650 cm^{-1} corresponding to Eg band, F2g and F2g become broad. When compared with the Raman spectra of pure Co_3O_4, in addition to the normal Raman bands, a new Raman band at ~315 cm^{-1} is seen for the catalyst $CoBi_2O_x$. For α-Bi_2O_3 synthesized on FTO, the prominent Raman bands are observed at ~215, 317, and 451 cm^{-1} which are attributed to Bi-O stretching mode (Figure S12).[48] However, none of these band features are seen in the Raman spectra of the Bi-doped cobalt oxides on FTO. Even in the case of $CoBi_2O_x$ which has a large amount of Bi, except for a new, broad Raman band at ~315 cm^{-1}, no sharp Raman peak associated with α-Bi_2O_3 is seen in its spectrum. These results obtained with Raman spectra indirectly confirm that Bi is present in cobalt oxide.

Next, the electrocatalytic activities of all the materials on FTO for OER in acidic solution (0.1 M $HClO_4$ solution with pH 1) are investigated using a three-electrode cell. In the cell, a calomel electrode is used as the reference electrode and a graphite rod is used as the counter electrode. To minimize the capacitive current, the polarization curves are obtained using a slow scan rate of 5 mV s^{-1}. The linear sweep voltammetry (LSV) curves, which are displayed in Figure 5a, show that the Bi-doped cobalt oxides have better electrocatalytic activities for OER in acidic solution compared with the pristine cobalt oxide. As the amount of Bi in cobalt oxide increases, its catalytic activity for OER also increases, with the highest activity being attained by the catalyst Co_9BiO_x (which has a Co:Bi ratio is 9:1). Further doping of Bi in cobalt oxide beyond this amount results in lower electrocatalytic activities in the materials. The Bi-doped cobalt oxide catalyst Co_9BiO_x, which is found to exhibit the best performance for OER in acidic solution, does so with the lowest overpotential (540 mV at a current density of 10 mA cm^{-2}). Meanwhile the highest overpotential (η = 671 mV) at a current density of 10 mA cm^{-2} is obtained for the pristine Co_3O_4. This means, all the Bi-doped cobalt oxide catalysts on FTO electrocatalyze the OER with lower overpotentials at a current density of 10 mA cm^{-2} than the pristine Co_3O_4 on FTO.

To determine the kinetics of OER in acidic media over these catalysts, their Tafel plots are generated from their respective LSV curves (Figure 5b). The lowest Tafel slope (113 mV dec^{-1}) is obtained for the catalyst Co_9BiO_x, indicating that the kinetics of OER on it is better than those of all the other catalysts studied here. The lowest

View Article Online
DOI: 10.1039/D4TA02845G

overpotential is also obtained for it, once again corroborating its high better electrocatalytic activity in acidic media. It is worth noting that even the catalyst $CoBi_2O_x$ (which has a Co:Bi ratio of 1:2 or more Bi than Co) exhibits a better catalytic performance for acidic OER with a lower overpotential (η = 646 mV) at a current density of 10 mA cm^{-2} than the pristine Co_3O_4 (η = 671 mV). This suggests that the Bi sites, along with Co atoms, in the former help the acidic OER catalysis. This is despite pristine Bi_2O_3 on FTO is inactive by itself for OER electrocatalysis in acidic solution, as can be seen from its LSV curve in Figure 5a. So, although Bi_2O_3 does not electrocatalyze OER, the Bi included in cobalt oxide substantially improve the overall electrocatalytic activity of the material for OER in acidic solution.

Next, the double-layer capacitances (C_{dl}) of the catalysts are determined based on the slopes of the linear plots of charging current density versus scan rate for the reactions over them (Figures 5d and S13). Note that the C_{dl} is directly proportional to the density of active sites on the surface of the catalysts exposed to the electrolyte. Among them, the value of C_{dl} of Co_9BiO_x is the highest. So, this catalyst must have the largest density of catalytically active sites on its surfaces, which may have been partly responsible for its best performance. In addition, compared with Co_3O_4, all the Bi-doped catalysts have higher values of C_{dl}, and thus larger density of electrochemically active sites to participate in the reaction. This is also in line with their better catalytic performances for OER than Co_3O_4. So, the incorporation of Bi in cobalt oxide increases the density of catalytically active sites on the surfaces of Co_3O_4, and thereby its electrocatalytic activity for OER.

We had to use the onset potentials and ECSA to compare our catalysts with one another, as mostly done for such catalysts, although their turnover frequencies (TOFs) would accurately reflect their intrinsic catalytic activity. However, it is not easy to determine the TOF of many types of electrocatalysts, especially multi-metallic and amorphous solid-state ones, like the ones reported here. This issue is widely discussed in a recent reference paper by Anantharaj et al.[49] The main reason is that the calculation of TOF requires an accurate number of active sites to normalize the measured activities with; however, methods to precisely determine their number for many electrocatalysts, like the ones here, are unavailable. The two most accurate methods used to determine the active sites on electrocatalysts are underpotential deposition (UPD) and redox peak integration. While the UPD method is more accurate for noble metals, the redox peak integration is applicable when the catalysts are monometallic. Additionally, since our catalysts have two active sites such as Co and Bi, precise calculation of the TOF values for each one is not possible using any available methods. To make the comparison easier, the same synthetic protocol and the same loading of catalysts on FTO substrates are employed. Furthermore, the morphologies of the catalysts obtained are almost the same, as evident from their SEM images. So, the geometrical surface areas of the catalysts should, at least, be similar for all of them. Indeed, the results of their double layer capacitance measurements (Figure 5d) show that the catalyst Co_9BiO_x has the highest density of active sites. So, its highest current density (see in Figure 5a) must be due to its highest density of active sites as its geometrical surface area is the same as those of the other catalysts. So, unsurprisingly, the catalyst with higher ECSA is found to have a higher overall electrocatalytic activity.

In the Nyquist plots obtained with EIS measurements, the diameters of the semicircles at high frequencies typically correspond to the interfacial charge transfer resistance (R_{ct}) of the electrocatalysts. As depicted in Figure 5e, the smallest semicircle or R_{ct} at higher frequencies is obtained for Co_9BiO_x, indicating its relatively favorable conductivity to enable more facile OER kinetics in acidic media. Additionally, the Nyquist plots show that Co_3O_4 has the highest R_{ct} among all Bi-doped cobalt oxide catalysts studied here. Not surprisingly, the overpotential of the electrocatalysts to drive OER increases from Co_9BiO_x to Co_3O_4. Even the electrocatalyst $CoBi_2O_x$, which has more Bi than Co, shows a better OER kinetics, or a lower value R_{ct}, than Co_3O_4. Additionally, $CoBi_2O_x$ has more density of active sites when compared to Co_3O_4. So, the results obtained with EIS corroborate that the incorporation of Bi in cobalt oxide enhances the electrochemical charge transfer processes over them during OER. This, and the higher density of catalytically active sites in $CoBi_2O_x$, is possible only if Bi itself also contributes to OER. In other words, although Bi in Bi_2O_3 is barely active for OER catalysis (Figure 5a), the Bi dopants incorporated into Co_3O_4 assist with the OER catalysis. Based on the results collectively, Co_9BiO_x, which has Co:Bi ratio of 9:1, is particularly found to exhibit the most facile OER kinetics, the lowest Tafel slope, the lowest interfacial charge transfer resistance, the highest density of active sites exposed on its surfaces, and the lowest overpotential to electrocatalyze the OER in acidic solution.

As one of the critical problems faced by most OER catalysts is that they are unstable under harsh acidic conditions, the stability of the Bi-doped cobalt oxide catalysts is also investigated with chronopotentiometry. The chronopotentiometric curve of the best catalyst, i.e., Co_9BiO_x, indicates that it remains stable at pH 1 for 45 hours and 24 h at current densities of 5 mA cm^{-2} and 10 mA cm^{-2}, respectively (Figure 5f). Its stability during acidic OER is also more robust compared to many notable non-noble acidic OER catalysts reported in the literature (see Table S4). Similarly, $Co_{14}BiO_x$ and Co_3O_4 are stable for 24 h under the same condition (Figure S14). However, the catalysts possessing more Bi, such as Co_2BiO_x and $CoBi_2O_x$, are not as stable.

Furthermore, the catalyst after the 5-hour stability test is analyzed by FESEM, EDS, and XPS. Its FESEM images (Figure S8) still show thin filament and petal morphologies even after 5 h of chronopotentiometric run, indicating its structural stability during catalysis. However, EDS and XPS analyses show that the Co:Bi ratios on the surfaces of the catalyst after 5 h of electrocatalytic stability test change from 7.2:1 and 8.3:1 to 22.5:1 and 14.8:1, respectively (Table S1 and S2). This means that after 5 hours long OER, this catalyst shows a relatively larger amount of Co than Bi on its surfaces. This indicates that Bi atoms on its surfaces may have leached into the electrolyte during the OER under such acidic solution, which is not uncommon for Bi. Nevertheless, the catalyst still functions reasonably well for at least 45 hours.

The XPS spectrum of the best catalyst Co_9BiO_x after the

View Article Online
DOI: 10.1039/D4TA02845G

chronopotentiometric OER test for 5 h is further analyzed to probe its active sites. Just like the deconvoluted Co 2p XPS spectra of pristine Co_9BiO_x, those of Co_9BiO_x after OER show peaks corresponding to Co^{2+} and Co^{3+} species (Figure S15a and Table S3). However, the relative ratio of Co^{2+}:Co^{3+} species on the surfaces of the catalyst increases from 3.14 to 3.44 after the OER, indicating that Co with an oxidation state of +2 is more favored during the OER (Table S1). Similarly, the Bi 4f XPS spectra of Co_9BiO_x before and after OER show that the relative ratio of Bi^{3+}:Bi^{5+} species changes from 2.39 to 3.42 after the OER (Figure S15b and Table S1 and S3). This indicates that some of the Bi^{3+} sites become Bi^{5+} during the OER. This change in the relative ratio of oxidation state of Bi also indirectly indicates Bi's participation during the electrocatalytic OER under such conditions. The deconvoluted O 1s XPS spectra of Co_9BiO_x after OER show peaks corresponding to the oxygen vacancies (with a binding energy at 530.69 eV) and the lattice oxygen (with a binding energy at 529.95 eV) as well as a peak at a binding energy of 531.48 eV, which can be ascribed to hydroxyl species, is seen (Figure S15c and Table S3). As the OER is done in acidic conditions, the latter must have formed due to the protonation of the catalyst surface and be among the intermediates formed during acidic OER.[7]

Since oxides of cobalt show reasonably good electrocatalytic activity towards OER, extensive studies have been conducted to determine the oxidation state of cobalt, i.e., Co^{2+} or Co^{3+}, that is more responsible for it.[50-53] In alkaline conditions, the studies showed that having more Co^{3+} in the catalyst improves the catalyst's activity for OER.[53, 54] However, in acidic conditions, Co^{2+}-rich Co_3O_4 has been found to do better as an OER catalytic site.[52] A recent report also corroborated that the high activity of Co^{2+} site towards acidic OER was due to the transformation of the Co^{2+}-O sites to reducible Co^{3+}-O sites in situ during the reaction, and its effect to facilitate the deprotonation of water and the release of dioxygen.[55] Note that these reducible Co^{3+}-O species forming in situ during OER have better activity for OER than the originally present Co^{3+}-O species on the catalyst. Additionally, studies have shown that the oxygen vacancies present on such catalysts can help with the in situ transformation of Co^{2+}-O species to Co^{3+}-O species.[55, 56] Based on these XPS results, the density of Co^{2+} species on the catalyst increases post OER. This means that the best catalyst Co_9BiO_x is rich with Co^{2+} species, which can translate to more oxygen vacancies as well as the presence of catalytically active sites favoring the OER. Furthermore, the oxygen vacancies can generate new bandgap states in the catalyst, which enhances the overall conductivity of the catalysts, thereby improving the OER catalytic performance.[22]

Since the densities of Bi^{3+} and Bi^{5+} species in the catalyst Co_9BiO_x have changed after OER, we believe that Bi in cobalt oxides also acts as the active site by forming Bi^{3+}/Bi^{5+} redox couple, as proposed for related materials in the literature.[33] Additional evidence on Bi acting as active site is found from electrochemical studies of $CoBi_2O_x$ catalyst. In this catalyst, the density of Co^{2+} species is less than that of Co^{3+} species, and the total amount of Bi (present in the form of both Bi^{3+} and Bi^{5+}) is more than the total amount of Co (in the form of both Co^{2+} and Co^{3+}). However, $CoBi_2O_x$ requires a lower overpotential and has a higher density of active sites than Co_3O_4, which has the highest density of Co^{2+} species. So, the improved catalytic performance exhibited by $CoBi_2O_x$ toward OER is possible

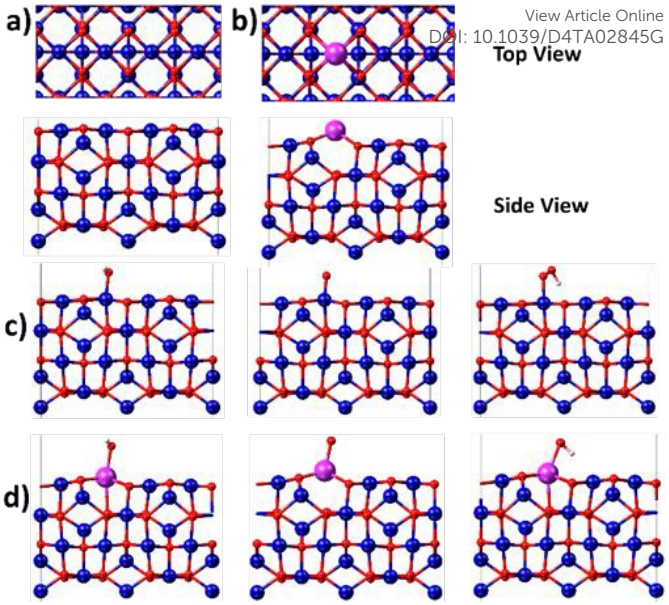

Figure 6. Top view and side view images of (a) Co_3O_4(100) surface and (b) Bi-doped Co_3O_4(100) surface. Red: oxygen, blue: cobalt, and purple: bismuth. Optimized structures of (c) Co_3O_4(100) surface and (d) Bi-doped Co_3O_4(100) surface, both with adsorbed *OH, *O, and *OOH intermediates.

only if Bi itself in the material catalyzes OER with an activity that is even better than that of Co. Pristine Bi_2O_3 is OER active only at potentials greater than ~2.0 V vs RHE[33] whereas $CoBi_2O_x$ is OER active at potentials greater than ~1.6 V vs RHE. This indicates that the Bi sites in $CoBi_2O_x$ are OER active at potentials below 2.0 V vs RHE. This enhancement in OER activity of Bi in $CoBi_2O_x$ than Bi in Bi_2O_3 can be attributed to the synergistic interaction between the Co and Bi species present in $CoBi_2O_x$ favoring catalysis. Based on our studies, while all Bi-doped cobalt oxides show higher electrocatalytic activities for OER in acidic condition, the optimal composition that does so the best is a Co:Bi ratio of 9:1 (or the material Co_9BiO_x). Bi's ability to improve the acidic OER activity of first-row transition metal oxides is apparently not limited to Co oxides, as our preliminary studies showed that Bi-doped iron oxides and nickel oxides also do the same. A detailed discussion on these two materials and their electrocatalytic properties are available in the Supporting Information.

Since the electrochemical studies point towards the possibility of Bi atoms contributing to the OER catalysis in acidic solutions, density functional theory (DFT) calculations are performed for the Bi-doped cobalt oxides catalysts. To do so, two catalyst slab models, namely Co_3O_4 (100) surface and Bi-doped Co_3O_4 (100) surface, are built as displayed in Figure 6a and 6b. Their optimized structures with adsorbed *OH, *O, and *OOH intermediates are depicted in Figure 6c-d. Their calculated free energy changes are shown in diagram presented in Figure 7. The results show that the ($H^+ + e^-$) transfer step with the largest free energy change value, represented with a bold line, is the potential determination step (PDS). The PDS of OER on Co_3O_4 (100) surface involves the conversion from *O to *OOH, resulting in an overpotential of 0.509 V. On the contrary, the PDS of

View Article Online
DOI: 10.1039/D4TA03845C

OER on Bi-doped Co_3O_4 (100) surface is the conversion from *OH to *O, leading to a calculated overpotential of 0.396 V. The energetic gap between *OH and *OOH is generally constant at 3.2 ± 0.2 eV due to the scaling relationship among different intermediates, which is observed not only for metallic catalysts but also for metal oxides.[8, 57, 58] Based on the theoretical studies, when Bi acts as the active site, the energy difference between the binding energies of *OH and *OOH for Bi-doped cobalt oxides is 2.56 eV, which is much lower than 3.2 eV. This shows that with the doping of Bi in cobalt oxide, the scaling relationship between *OH and *OOH can be broken, making the catalyst require a lower overpotential to drive OER. This suggests that the incorporation of Bi is beneficial for promoting the OER in acidic solutions.

As a final note, Bi is also found to improve the electrocatalytic activities of iron oxides and nickel oxides for OER in acidic conditions. However, the stabilities of both these materials are much inferior to the Bi-doped cobalt oxides. The results and the pertinent discussions on these materials are presented in the Supporting Information and Figures S16-19.

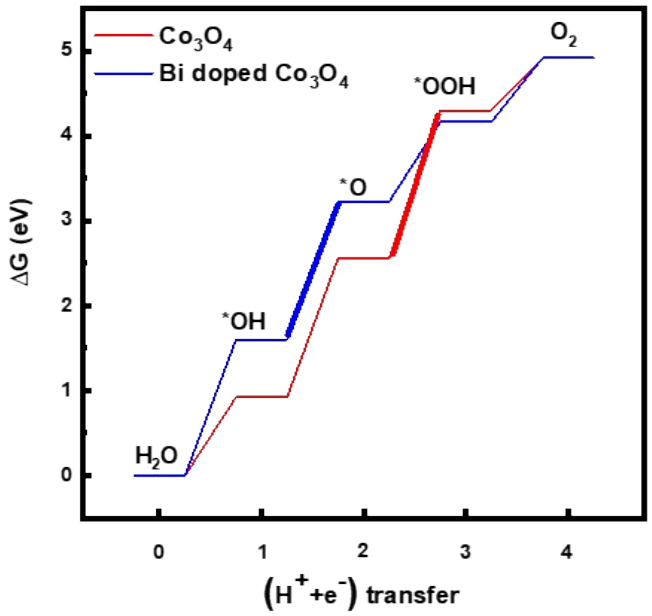

Figure 7. Calculated free energy change diagrams of OER on the surface of Co_3O_4(100) and Bi-doped Co_3O_4.

3. Conclusions

In summary, cobalt oxides doped with the p-block metal Bi in different ratios of Co:Bi, which have thin filament and petal-like morphologies, were synthesized in situ on FTO substrates using a simple procedure. The materials showed high durability and catalytic activity for acidic OER. Upon investigating the catalysts synthesized with different Co:Bi ratios, the one with a Co:Bi ratio of 9:1 (Co_9BiO_x) was found to be the most optimal to exhibit the best performance for acidic OER, with an overpotential of 540 mV at the current density of 10 mA cm^{-2}. This catalyst was also found to be stable for more than 24 h while driving the reaction at a current density of 5 mA cm^{-2}. XRD patterns showed that the addition of Bi into cobalt oxide renders them more active acidic OER electrocatalysts. The SEM images of the resulting Bi-doped cobalt oxides revealed that their morphologies would change from thin filament and petal-like morphology to sheet-like structures as the amount of Bi in the catalysts was increased. The XPS studies of the catalysts before and after OER indicated that the relative ratios of the metallic species, namely, Co^{2+}:Co^{3+} and Bi^{3+}:Bi^{5+}, on the surfaces of the catalysts changed, indirectly revealing that both Co and Bi could serve as the active sites during OER. DFT calculations also corroborated that Bi doped into cobalt oxide would help with the catalytic activity of the material for OER, lowering the overpotential of the reaction. In addition, Bi was found to enhance the electrocatalytic activities of iron oxides and nickel oxides for OER in acidic conditions. These results collectively show that the p-block metal Bi, which is underexplored for electrocatalysis, holds a great potential for producing acid stable, high performing OER catalysts. We believe that our findings will further inspire more research on main group metals towards the development of acidic OER catalysts.

Author Contributions

B.T. and B.P. contributed equally to the work. B.T. and B.P. conducted most of the experiments and the synthesis and characterization of the catalysts, and X.H conducted the DFT studies on the catalysts. B.T., B.P., and T.A. conceived the study. T.A. supervised the study and provided the resources. B.T., T.A., and X.H. wrote the draft paper. B.T. and T.A. reviewed and revised the paper. T.A. submitted the paper. All authors discussed the results and commented on the manuscript.

Conflicts of interest

There are no conflicts to declare in this work and report.

Acknowledgements

We thank Ann Mary Jose and Prof. Ashutosh Goel for their assistance with elemental analysis to cross-check some of the samples in this work, the results of which ultimately ended up not relevant and thus not included.

Data Availability Statement

Data for this article, including materials characterizations, electrochemical and electrocatalytic test results, and DFT calculations, are available the authors' computers and university instrumentation computers. Some of the data supporting this article have been included as part of the Supplementary Information.

Notes and references

1. Byrne, B.; Liu, J.; Bowman, K.; Pascolini-Campbell, M.; Chatterjee, A.; Pandey, S.; Miyazaki, K.; Werf, G. V. D.; Wunch, D.; Wennberg, P.; Roehl, C.; Sinha, S. *Unprecedented Canadian forest fire carbon emissions during 2023*; In Review: DOI: https://doi.org/10.21203/rs.3.rs-3684305/v1.
2. Wang, Z.; Wang, Z.; Zou, Z.; Chen, X.; Wu, H.; Wang, W.; Su, H.; Li, F.; Xu, W.; Liu, Z.; Zhu, J., Severe Global Environmental Issues

Caused by Canada's Record-Breaking Wildfires in 2023. *Advances in Atmospheric Sciences* **2023**.
3. Chatenet, M.; Pollet, B. G.; Dekel, D. R.; Dionigi, F.; Deseure, J.; Millet, P.; Braatz, R. D.; Bazant, M. Z.; Eikerling, M.; Staffell, I.; Balcombe, P.; Shao-Horn, Y.; Schäfer, H., Water electrolysis: from textbook knowledge to the latest scientific strategies and industrial developments. *Chemical Society Reviews* **2022,** *51* (11), 4583-4762.
4. Gao, J.; Tao, H.; Liu, B., Progress of Nonprecious-Metal-Based Electrocatalysts for Oxygen Evolution in Acidic Media. *Advanced Materials* **2021,** *33* (31), 2003786.
5. Grigoriev, S. A.; Fateev, V. N.; Bessarabov, D. G.; Millet, P., Current status, research trends, and challenges in water electrolysis science and technology. *International Journal of Hydrogen Energy* **2020,** *45* (49), 26036-26058.
6. Feng, Q.; Yuan, X. Z.; Liu, G.; Wei, B.; Zhang, Z.; Li, H.; Wang, H., A review of proton exchange membrane water electrolysis on degradation mechanisms and mitigation strategies. *Journal of Power Sources* **2017,** *366*, 33-55.
7. Li, L.; Wang, P.; Shao, Q.; Huang, X., Recent Progress in Advanced Electrocatalyst Design for Acidic Oxygen Evolution Reaction. *Advanced Materials* **2021,** *33* (50), 2004243.
8. An, L.; Wei, C.; Lu, M.; Liu, H.; Chen, Y.; Scherer, G. G.; Fisher, A. C.; Xi, P.; Xu, Z. J.; Yan, C. H., Recent Development of Oxygen Evolution Electrocatalysts in Acidic Environment. *Adv Mater* **2021,** *33* (20), e2006328.
9. Blasco-Ahicart, M.; Soriano-López, J.; Carbó, J. J.; Poblet, J. M.; Galan-Mascaros, J. R., Polyoxometalate electrocatalysts based on earth-abundant metals for efficient water oxidation in acidic media. *Nature Chemistry* **2018,** *10* (1), 24-30.
10. Niu, S.; Kong, X.-P.; Li, S.; Zhang, Y.; Wu, J.; Zhao, W.; Xu, P., Low Ru loading RuO2/(Co,Mn)3O4 nanocomposite with modulated electronic structure for efficient oxygen evolution reaction in acid. *Applied Catalysis B: Environmental* **2021,** *297*, 120442.
11. Huynh, M.; Ozel, T.; Liu, C.; Lau, E. C.; Nocera, D. G., Design of template-stabilized active and earth-abundant oxygen evolution catalysts in acid. *Chemical Science* **2017,** *8* (7), 4779-4794.
12. Li, A.; Ooka, H.; Bonnet, N.; Hayashi, T.; Sun, Y.; Jiang, Q.; Li, C.; Han, H.; Nakamura, R., Stable Potential Windows for Long-Term Electrocatalysis by Manganese Oxides Under Acidic Conditions. *Angewandte Chemie International Edition* **2019,** *58* (15), 5054-5058.
13. Frydendal, R.; Paoli, E. A.; Chorkendorff, I.; Rossmeisl, J.; Stephens, I. E. L., Toward an Active and Stable Catalyst for Oxygen Evolution in Acidic Media: Ti-Stabilized MnO_2. *Advanced Energy Materials* **2015,** *5* (22), 1500991.
14. Zhao, W.; Xu, F.; Yang, J.; Hu, X.; Weng, B., Ce Single-Atom Incorporation Enhances the Oxygen Evolution Reaction of Co3O4 in Acid. *Inorganic Chemistry* **2024,** *63* (4), 1947-1953.
15. Fan, R.-Y.; Zhao, H.-Y.; Zhen, Y.-N.; Wang, F.-G.; Hu, H.; Chai, Y.-M.; Dong, B., Mn-induced strengthening hybridization effect of Co–O bond for stable oxygen evolution in acidic media. *Fuel* **2023,** *333*, 126361.
16. Etzi Coller Pascuzzi, M.; van Velzen, M.; Hofmann, J. P.; Hensen, E. J. M., On the Stability of Co_3O_4 Oxygen Evolution Electrocatalysts in Acid. *ChemCatChem* **2021,** *13* (1), 459-467.
17. Li, A.; Kong, S.; Guo, C.; Ooka, H.; Adachi, K.; Hashizume, D.; Jiang, Q.; Han, H.; Xiao, J.; Nakamura, R., Enhancing the stability of cobalt spinel oxide towards sustainable oxygen evolution in acid. *Nature Catalysis* **2022,** *5* (2), 109-118.
18. Sun, L.; Feng, M.; Peng, Y.; Zhao, X.; Shao, Y.; Yue, X.; Huang, S., Constructing oxygen vacancies by doping Mo into spinel Co_3O_4 to trigger a fast oxide path mechanism for acidic oxygen evolution reaction. *Journal of Materials Chemistry A* **2024**.
19. Zhu, Y.; Wang, J.; Koketsu, T.; Kroschel, M.; Chen, J.-M.; Hsu, S.-Y.; Henkelman, G.; Hu, Z.; Strasser, P.; Ma, J., Iridium single atoms incorporated in Co_3O_4 efficiently catalyze the oxygen evolution in acidic conditions. *Nature Communications* **2022,** *13* (1), 7754.
20. Yan, K.-L.; Chi, J.-Q.; Xie, J.-Y.; Dong, B.; Liu, Z.-Z.; Gao, W.-K.; Lin, J.-H.; Chai, Y.-M.; Liu, C.-G., Mesoporous Ag-doped Co_3O_4 nanowire arrays supported on FTO as efficient electrocatalysts for oxygen evolution reaction in acidic media. *Renewable Energy* **2018,** *119*, 54-61.
21. Yang, X.; Li, H.; Lu, A.-Y.; Min, S.; Idriss, Z.; Hedhili, M. N.; Huang, K.-W.; Idriss, H.; Li, L.-J., Highly acid-durable carbon coated Co_3O_4 nanoarrays as efficient oxygen evolution electrocatalysts. *Nano Energy* **2016,** *25*, 42-50.
22. Lai, Q.; Vediyappan, V.; Aguey-Zinsou, K.-F.; Matsumoto, H., One-Step Synthesis of Carbon-Protected Co_3O_4 Nanoparticles toward Long-Term Water Oxidation in Acidic Media. *Advanced Energy and Sustainability Research* **2021,** *2* (11), 2100086.
23. Tran-Phu, T.; Chen, H.; Daiyan, R.; Chatti, M.; Liu, B.; Amal, R.; Liu, Y.; Macfarlane, D. R.; Simonov, A. N.; Tricoli, A., Nanoscale TiO_2 Coatings Improve the Stability of an Earth-Abundant Cobalt Oxide Catalyst during Acidic Water Oxidation. *ACS Applied Materials & Interfaces* **2022,** *14* (29), 33130-33140.
24. Wang, Z.; Zheng, Y.-R.; Chorkendorff, I.; Nørskov, J. K., Acid-Stable Oxides for Oxygen Electrocatalysis. *ACS Energy Letters* **2020,** *5* (9), 2905-2908.
25. Han, B.; Risch, M.; Belden, S.; Lee, S.; Bayer, D.; Mutoro, E.; Shao-Horn, Y., Screening Oxide Support Materials for OER Catalysts in Acid. *Journal of The Electrochemical Society* **2018,** *165* (10), F813.
26. Gunasooriya, G. T. K. K.; Nørskov, J. K., Analysis of Acid-Stable and Active Oxides for the Oxygen Evolution Reaction. *ACS Energy Letters* **2020,** *5* (12), 3778-3787.
27. Vallez, L.; Jimenez-Villegas, S.; Garcia-Esparza, A. T.; Jiang, Y.; Park, S.; Wu, Q.; Gill, T. M.; Sokaras, D.; Siahrostami, S.; Zheng, X., Effect of doping TiO2 with Mn for electrocatalytic oxidation in acid and alkaline electrolytes. *Energy Advances* **2022,** *1* (6), 357-366.
28. Zhao, L.; Cao, Q.; Wang, A.; Duan, J.; Zhou, W.; Sang, Y.; Liu, H., Iron oxide embedded titania nanowires – An active and stable electrocatalyst for oxygen evolution in acidic media. *Nano Energy* **2018,** *45*, 118-126.
29. Anantharaj, S.; Karthick, K.; Kundu, S., Spinel Cobalt Titanium Binary Oxide as an All-Non-Precious Water Oxidation Electrocatalyst in Acid. *Inorganic Chemistry* **2019,** *58* (13), 8570-8576.
30. Wang, J.; Kim, H.; Lee, H.; Ko, Y.-J.; Han, M. H.; Kim, W.; Baik, J. M.; Choi, J.-Y.; Oh, H.-S.; Lee, W. H., Sb incorporated into oxides enhances stability in acid during the oxygen evolution reaction by inhibiting structural distortion. *Nano Energy* **2023,** *110*, 108355.
31. Evans, T. A.; Choi, K.-S., Electrochemical Synthesis and Investigation of Stoichiometric, Phase-Pure $CoSb_2O_6$ and MnSb2O6 Electrodes for the Oxygen Evolution Reaction in Acidic Media. *ACS Applied Energy Materials* **2020,** *3* (6), 5563-5571.
32. Wang, Y.; Zhao, H.; Guo, Y.; Wu, J.; Lu, X.; Tang, X., Pyrochlore-type cobalt and manganese antimonate electrocatalysts with

excellent activity and stability for OER in acidic solution. *Nanoscale* **2023,** *15* (21), 9413-9422.

33. Thorarinsdottir, A. E.; Costentin, C.; Veroneau, S. S.; Nocera, D. G., p-Block Metal Oxide Noninnocence in the Oxygen Evolution Reaction in Acid: The Case of Bismuth Oxide. *Chemistry of Materials* **2022,** *34* (2), 826-835.
34. Simondson, D.; Chatti, M.; Gardiner, J. L.; Kerr, B. V.; Hoogeveen, D. A.; Cherepanov, P. V.; Kuschnerus, I. C.; Nguyen, T. D.; Johannessen, B.; Chang, S. L. Y.; MacFarlane, D. R.; Hocking, R. K.; Simonov, A. N., Mixed Silver–Bismuth Oxides: A Robust Oxygen Evolution Catalyst Operating at Low pH and Elevated Temperatures. *ACS Catalysis* **2022,** *12* (20), 12912-12926.
35. Du, H.-L.; Chatti, M.; Kerr, B.; Nguyen, C. K.; Tran-Phu, T.; Hoogeveen, D. A.; Cherepanov, P. V.; Chesman, A. S. R.; Johannessen, B.; Tricoli, A.; Hocking, R. K.; MacFarlane, D. R.; Simonov, A. N., Durable Electrooxidation of Acidic Water Catalysed by a Cobalt-Bismuth-based Oxide Composite: An Unexpected Role of the F-doped SnO2 Substrate. *ChemCatChem* **2022,** *14* (11), e202200013.
36. Thomas, B.; Tang, C.; Ramírez-Hernández, M.; Asefa, T., Incorporation of Bismuth Increases the Electrocatalytic Activity of Cobalt Borates for Oxygen Evolution Reaction. *ChemPlusChem* **2023,** *88* (5), e202300104.
37. Wang, H.-Y.; Hung, S.-F.; Chen, H.-Y.; Chan, T.-S.; Chen, H. M.; Liu, B., In Operando Identification of Geometrical-Site-Dependent Water Oxidation Activity of Spinel Co_3O_4. *Journal of the American Chemical Society* **2016,** *138* (1), 36-39.
38. Ollevier, T.; Jalba, A.; Keipour, H., Bismuth(III) Nitrate Pentahydrate. In *Encyclopedia of Reagents for Organic Synthesis (EROS)*, 2016; pp 1-9.
39. Irmawati, R.; Noorfarizan Nasriah, M. N.; Taufiq-Yap, Y. H.; Abdul Hamid, S. B., Characterization of bismuth oxide catalysts prepared from bismuth trinitrate pentahydrate: influence of bismuth concentration. *Catalysis Today* **2004,** *93-95*, 701-709.
40. Younis, A.; Chu, D.; Lin, X.; Lee, J.; Li, S., Bipolar resistive switching in p-type Co_3O_4 nanosheets prepared by electrochemical deposition. *Nanoscale Research Letters* **2013,** *8* (1), 36.
41. Zhang, Q.; Yang, P.; Zhang, H.; Zhao, J.; Shi, H.; Huang, Y.; Yang, H., Oxygen vacancies in Co_3O_4 promote CO_2 photoreduction. *Applied Catalysis B: Environmental* **2022,** *300*, 120729.
42. Wang, J.; Gao, R.; Zhou, D.; Chen, Z.; Wu, Z.; Schumacher, G.; Hu, Z.; Liu, X., Boosting the Electrocatalytic Activity of Co3O4 Nanosheets for a Li-O2 Battery through Modulating Inner Oxygen Vacancy and Exterior Co^{3+}/Co^{2+} Ratio. *ACS Catalysis* **2017,** *7* (10), 6533-6541.
43. Xu, W.; Lyu, F.; Bai, Y.; Gao, A.; Feng, J.; Cai, Z.; Yin, Y., Porous cobalt oxide nanoplates enriched with oxygen vacancies for oxygen evolution reaction. *Nano Energy* **2018,** *43*, 110-116.
44. Gautam, S.; Aggarwal, V.; Singh, B.; Awana, V. P. S.; Ganesan, R.; Kushvaha, S. S., Signature of weak-antilocalization in sputtered topological insulator Bi_2Se_3 thin films with varying thickness. *Scientific Reports* **2022,** *12* (1), 9770.
45. Zhang, Y.; Feng, L.; Zhan, W.; Li, S.; Li, Y.; Ren, X.; Zhang, P.; Sun, L., Co_3O_4 Hollow Porous Nanospheres with Oxygen Vacancies for Enhanced Li–O2 Batteries. *ACS Applied Energy Materials* **2020,** *3* (4), 4014-4022.
46. Wang, Z.; Wang, W.; Zhang, L.; Jiang, D., Surface oxygen vacancies on Co3O4 mediated catalytic formaldehyde oxidation at room temperature. *Catalysis Science & Technology* **2016,** *6* (11), 3845-3853.
47. Wang, Y.; Zhu, Y.-Q.; Xie, Z.; Xu, S.-M.; Xu, M.; Li, Z.; Ma, L.; Ge, R.; Zhou, H.; Li, Z.; Kong, X.; Zheng, L.; Zhou, J.; Duan, H., Efficient Electrocatalytic Oxidation of Glycerol via Promoted OH* Generation over Single-Atom-Bismuth-Doped Spinel Co_3O_4. *ACS Catalysis* **2022,** *12* (19), 12432-12443.
48. Wang, X.; He, W.; Shi, J.; Junqueira, J. R. C.; Zhang, J.; Dieckhöfer, S.; Seisel, S.; Das, D.; Schuhmann, W., Ag-induced Phase Transition of Bi_2O_3 Nanofibers for Enhanced Energy Conversion Efficiency towards Formate in CO_2 Electroreduction. *Chemistry – An Asian Journal* **2023,** *18* (2), e202201165.
49. Anantharaj, S.; Karthik, P. E.; Noda, S., The Significance of Properly Reporting Turnover Frequency in Electrocatalysis Research. *Angewandte Chemie International Edition* **2021,** *60* (43), 23051-23067.
50. Ya, M.; Wang, J.; Li, G.; Gao, G.; Zhao, X.; Cui, J.; Wu, H.; Li, L., Surface Engineering in $MgCo_3O_4$ Spinel Oxide for an Improved Oxygen Evolution Reaction. *ACS Sustainable Chemistry & Engineering* **2023,** *11* (2), 744-750.
51. Xu, Y.; Zhang, F.; Sheng, T.; Ye, T.; Yi, D.; Yang, Y.; Liu, S.; Wang, X.; Yao, J., Clarifying the controversial catalytic active sites of Co_3O_4 for the oxygen evolution reaction. *Journal of Materials Chemistry A* **2019,** *7* (40), 23191-23198.
52. Yan, K.-L.; Qin, J.-F.; Lin, J.-H.; Dong, B.; Chi, J.-Q.; Liu, Z.-Z.; Dai, F.-N.; Chai, Y.-M.; Liu, C.-G., Probing the active sites of Co_3O_4 for the acidic oxygen evolution reaction by modulating the Co^{2+}/Co^{3+} ratio. *Journal of Materials Chemistry A* **2018,** *6* (14), 5678-5686.
53. Han, X.; He, G.; He, Y.; Zhang, J.; Zheng, X.; Li, L.; Zhong, C.; Hu, W.; Deng, Y.; Ma, T.-Y., Engineering Catalytic Active Sites on Cobalt Oxide Surface for Enhanced Oxygen Electrocatalysis. *Advanced Energy Materials* **2018,** *8* (10), 1702222.
54. Alex, C.; Sarma, S. C.; Peter, S. C.; John, N. S., Competing Effect of Co^{3+} Reducibility and Oxygen-Deficient Defects Toward High Oxygen Evolution Activity in Co_3O_4 Systems in Alkaline Medium. *ACS Applied Energy Materials* **2020,** *3* (6), 5439-5447.
55. Liu, J.; Wang, T.; Liu, X.; Shi, H.; Li, S.; Xie, L.; Cai, Z.; Han, J.; Huang, Y.; Wang, G.; Li, Q., Reducible Co^{3+}–O Sites of Co–Ni–P–Ox on CeO_2 Nanorods Boost Acidic Water Oxidation via Interfacial Charge Transfer-Promoted Surface Reconstruction. *ACS Catalysis* **2023,** *13* (8), 5194-5204.
56. Bergmann, A.; Jones, T. E.; Martinez Moreno, E.; Teschner, D.; Chernev, P.; Gliech, M.; Reier, T.; Dau, H.; Strasser, P., Unified structural motifs of the catalytically active state of Co(oxyhydr)oxides during the electrochemical oxygen evolution reaction. *Nature Catalysis* **2018,** *1* (9), 711-719.
57. Rossmeisl, J.; Qu, Z. W.; Zhu, H.; Kroes, G. J.; Nørskov, J. K., Electrolysis of water on oxide surfaces. *Journal of Electroanalytical Chemistry* **2007,** *607* (1), 83-89.
58. Man, I. C.; Su, H.-Y.; Calle-Vallejo, F.; Hansen, H. A.; Martínez, J. I.; Inoglu, N. G.; Kitchin, J.; Jaramillo, T. F.; Nørskov, J. K.; Rossmeisl, J., Universality in Oxygen Evolution Electrocatalysis on Oxide Surfaces. *ChemCatChem* **2011,** *3* (7), 1159-1165.

View Article Online
DOI: 10.1039/D4TA02845G

Data Availability Statement

Data for this article, including materials characterizations, electrochemical and electrocatalytic test results, and DFT calculations, are available the authors' computers and university instrumentation computers. Some of the data supporting this article have been included as part of the Supplementary Information.